Cement and Concrete Research 42 (2012) 745–751

Contents lists available at SciVerse ScienceDirect

Cement and Concrete Research

journal homepage: http://ees.elsevier.com/CEMCON/default.asp

Effects of aggregate size on alkali–silica-reaction induced expansion

Cyrille F. Dunant [a,*], Karen L. Scrivener [b]

[a] University of Toronto, Galbraith Building, 35 St. George street, Toronto, Canada M5S 1A4
[b] EPFL STI IMX LMC, MXG 232 (BÃ¢timent MXG), Station 12, CH-1015 Lausanne, Switzerland

ARTICLE INFO

Article history:
Received 19 March 2011
Accepted 17 February 2012

Keywords:
Alkali-Aggregate Reaction (ASR) (C)
XFEM
Long-Term Performance (C)
Mechanical properties (C)
Modelling (E)

ABSTRACT

The macroscopic effects of ASR are linked to the damage state at the microstructure level. In this paper we used a combination of experiments and modelling to study the effect of aggregate size on the manifestation of ASR. There are two main ways in which the size of the aggregates can affect damage evolution: the propagation of cracks in aggregates of different sizes and the interactions between expanding and non-expanding aggregates in a densely packed microstructure. To assess these effects, concretes were cast with the same PSD but each with a different size class of reactive aggregates. Numerical simulations were used to model the mechanical interactions in single aggregates and in complete microstructures at the mesoscopic level. From the simulations a mechanism is proposed to explain the experimental observations. This suggests that: the expansion rate of ASR affected concrete depends on the fracture behaviour of individual aggregates in the early stage, and on the fracture behaviour of the paste in the later stages.

1. Introduction

Due to constraints in terms of storage and faster kinetics, laboratory samples made for the purpose of testing cementitious materials affected by ASR are mortars or concrete mixes with a fairly small maximum aggregate size. However, it has been observed that the PSD of the aggregates has an influence on the kinetics and amount of expansion. Therefore extrapolation to real PSDs is required to use the laboratory results for field prediction. Such extrapolation is made difficult because the effects of the PSD are complex. In this study, experiments and numerical simulations are combined to better understand the impact of aggregate size on the manifestation of ASR.

2. Literature background

The effect of aggregate size and amount has been previously studied and this has led to recommendations which specify correction factors to extrapolate from laboratory specimens to field structures. The size effect can be understood as the effect of the partial contributions of the different size fractions. Both parameters have been reported to either increase or decrease the expansion, and no satisfactory mechanism has been proposed to explain the experimental observations.

Experimental work on different size fractions has mostly been done in mortars, which encompass a relatively narrow range of sizes. Poyet studied the effect of different reactive size fractions [1]. He found that very fine fractions do not cause expansion. His results mirror that of the landmark paper from Stanton in 1940 [24]. Cyr and colleagues performed a similar study with finely ground reactive aggregates of various types, and found they all reduced the expansion [2]. The aggregate used by Poyet was a very reactive flint, and the results could be explained by a pozzolanic reaction of the fine reactive particles, as also proposed by Cyr and colleagues, who performed a similar study on mortar. They tried to determine the effect of angularity as well as size, but their "natural" and crushed aggregates are of a different mineralogical nature. The fractions with the least expansive effect were the smallest and largest, namely 0.125–0.25 and 2–4 mm [3].

Zhang and co-workers studied the influence of the large aggregate content in a concrete mix where all the aggregates were reactive [4]. They found that depending on the reactivity of the aggregate the overall effect of larger aggregates could be either a reduction or an increase of the measured macroscopic expansion. This confirmed earlier reports by French [5] who found that the most deleterious fraction in terms of expansion was the 4–10 mm fraction. The general trend however is that the presence of larger aggregates reduces expansion at early age, and increases it later. For example, in the Norwegian recommendations [6], the expansion from large aggregates in accelerated tests is multiplied by a factor greater than one to account for the enhanced expansion potential at later ages.

Wiggum and colleagues first considered the role of grading by comparing the relative surface of model fully reactive aggregates [7]. However, in discussing accelerated tests, they found that variations of the amount of reactive material in each class have a relatively small effect on the total expansion [8]. This observation is incompatible with the theory that ASR occurs mainly at the surface of aggregates as the surface of differently sized aggregates in contact with the paste varies considerably.

* Corresponding author. Tel.: +1 416 978 7863; fax: +1 416 978 2077.
E-mail address: cyrille.dunant@gmail.com (C.F. Dunant).

0008-8846/$ – see front matter © 2012 Elsevier Ltd. All rights reserved.
doi:10.1016/j.cemconres.2012.02.012

An analytical model, based on the development of reaction rims was published by BaÅ¾ant [9], which takes into account the interactions between aggregates to explain the shape of the expansion curve. Attempts to integrate the effect of individual fractions in ASR models have been made. Notably, Multon has proposed an ASR model which considers the expansion of the aggregate classes separately [10]. However, these models assume that aggregates react on the surface. As the aggregate content to aggregate surface ratio is highly dependent on the grading, different reactivities for each class need to be assumed.

Mechanical explanations for size-dependant factors have been proposed: Dunant, in his thesis, reproduced the expansion curves of concretes produced with different particle size distribution. This approach, which is the same one as in this paper, is based on micro-mechanical modelling of the damage in numerical microstructures [11]. It has been suggested that the splitting of individual aggregates is a driving mechanism behind the differences in expansion kinetics when different gradations are used: in a recent analytical analysis, Reinhardt and Mielich calculated the critical crack length for aggregate failure, which is size dependant, but do not consider the crack network formed in the aggregates [12].

In general, the observed effected of aggregate size on the ASR-induced expansion could be due to various causes of either chemical or mechanical origin:

- Different mineralogy of aggregates at different sizes. Different aggregates could be assumed to have different reactivities and fracture properties. However, size effects can be observed even when all aggregates have the same mineralogy. Furthermore, in the studies cited above, when a single class of aggregate is reactive, it is usually obtained by crushing a single aggregate type. Ramyar et al. studied whether differences came from the process of crushing, but found that it only increased dispersion between the samples [3].
- Diffusion process of the alkalies or water to the core of larger aggregates. For example, in his model, Bažant uses the diffusion of water as a controlling kinetic parameter — alkali ions are very mobile, and should reach the reactive sites too fast for this to have a significant effect. However, size effects have been observed even for aggregates with significant initial cracking [11].
- Fracture mechanics effects of the forces exerted by aggregates on their neighbours and the different crack propagation lengths in aggregates as a function of their size, such as described by Reinhardt and Mielich. This is the mechanism which is expected to be dominant, and which is explored in more details in this paper.

All these effects are not necessarily mutually exclusive and could also happen simultaneously. This paper focuses on the fracture mechanics-based size effects at the aggregate level, and how they can explain the different expansive properties of different size fractions of aggregates.

3. Methods and numerical model

In this study, two aggregates were used. The first was an aggregate known to be reactive and used in the previously reported work Ben Haha and colleague [13]. The other was non-reactive. Both aggregates are mixed-mineralogy alpine aggregates, but the reactive aggregate consists mostly of chloritic schist, the mineralogy of which is described in Ben Haha's thesis. Both aggregates were crushed sieved and then separated into different size fractions as listed in Table 1.

All mixes prepared in this study follow the Bolomey reference curves [14], composed from the fractions prepared. The aggregates for all mixes were well homogenised prior to mixing to ensure a homogeneous blend. Approximately 72% of the volume of the concrete was aggregates.

All mixes were prepared with CEM I cement coming from a single batch to which was added 0.8 wt.% of NaOH dissolved in the mix water. A water to cement ratio of 0.43 was used. The mix designs are reported in Table 2.

Table 1
List of sieves used for the separation of the reactive aggregates. The separations indicate the cut-off points for the general classes used. The percentages reported are for the classes of the control aggregate.

Opening in mm	0–2	2–4	4–8	8–16
0.053	5.5		1.5	1.2
0.063	7.3		1.5	1.2
0.10	15.6		1.5	1.2
0.16	10.0		1.5	1.2
0.25	22.0		1.5	1.2
0.40	34.3		1.5	1.2
0.63	53.0		1.5	1.2
1.0	76.3		1.5	1.2
1.6	100.0		2.8	1.2
2.5		48.5	4.4	1.2
4.0		93.8	14.3	1.2
5.0		100.0	40.6	1.2
6.3			66.7	1.5
8.0			91.3	3.6
10.0			99.7	20.9
12.5			100.0	66.3
16.0				97.2
20.0				100.0
25.0				

3.1. Methods

Prismatic concrete samples of $7 \times 7 \times 28$ cm were prepared with embedded stainless steel studs. Three samples were prepared for each experimental condition. The experiments designed to study the effect of the individual fractions required preparation of the reactive aggregates. To ensure that the reactive and non-reactive mixes had the same PSD the sub-fractions were recomposed to match those of the non-reactive control as described above. As all reactive fractions were prepared from aggregates originally from the same class, the fraction of reactive material in each class is constant. A table of all samples cast for this purpose is provided below (Table 3).

All samples were cast using the following protocol: aggregates and cement were mixed together at low speed for 1 min. During the next minute, water and sodium hydroxide were added to the mix. Mixing was continued for 2 min at high speed. Moulds were filled in two stages with intermediate vibration. The concrete surface was smoothed and the samples were immediately placed in humid conditions. At 24 h, all samples were demoulded and placed in a fog room for a further 28Â day cure. After this initial cure, the samples were placed in 0.150 mol/l alkaline solutions at 38 °C. Regular measures were performed at 20 °C, each after a 24 h cool-down period.

Rather than storage in 100% relative humidity conditions, the samples were stored in simulated pore solutions. In 100% relative humidity conditions it is difficult to avoid leaching due to condensation and the results may show variability due to difficulties in controlling the saturation state.

Even when the samples are kept in small quantities of water, it is not possible to prevent leaching from occurring. Therefore NaOH was

Table 2
Mix design for the mortars and concretes. The aggregates were all prepared so the 0–0.0125 mm class had been removed.

Material	Note	Concrete batch
Cement	Holcim Pur 4	11,700 g
Water	Tap water	5000 g
Aggregate		48,000 g
Sodium hydroxide	Mixed with water to reach 0.8 wt.% alkali cement mass	46 g
Superplasticizer	Rheobuild 5550	92 g

Table 3
Mixes from partly reactive aggregates.

Fraction	0–2	2–4	4–8	8–16	wt.%
Reactive	**Yes**	No	No	No	32
Reactive	No	**Yes**	No	No	16
Reactive	No	No	**Yes**	No	29
Reactive	No	No	No	**Yes**	21

added to the cure water to reflect the concentration in the cement pore solution (0.150 mol/l). The concentration in Na^+ in cement pore solutions has been measured in the literature between 50 mmol/l and 100 mmol/l, and the concentration of K^+ at around 550 mmol/l [15]. To minimise leaching, whether from the paste to the curing solution or in the other direction, the solutions should have the same composition. However, using too much alkalis can induce non-linear effects on the expansion. As a compromise, the curing solution was a concentration at the low end of what is described in the literature, so that leaching is minimised, but the reaction is not otherwise affected.

3.2. Numerical model

3.2.1. Geometrical setup

AMIE [16–18] was used to simulate ASR-affected concrete. Simulations were made with single aggregates and with complete microstructures taking into account all the grains in a slice [19,20]. To reproduce the interactions between the different aggregate classes in the 2D simulations, each aggregate in a generated PSD is transformed to its expected diameter in a slice. This produce a slice with the same PSD as a slice from a 3D microstructure, but with better control of the inter-aggregate spacing. This way, the PSD in the 2D setup is equivalent to the one in the 3D in terms of neighbourhoods of differently sized aggregates. Furthermore, the same proportion of expansion comes from the same aggregate class, as the proportions of the different fractions are kept, and the effects of size and in-aggregate crack propagation are reproduced in the sections (Fig. 1). In the simulations, the sample size was 70×70 mm for the concretes. This size is sufficient for the numerical samples to be representative. As the samples are the same size as the experimental samples, the boundary conditions were not set to be periodic: only a pin and a roller inhibit the free body movement of the samples, which is otherwise free to deform.

As previously described in [17], and consistent with microstructural observations [11,13], ASR gel production is modelled as expanding inclusions homogeneously dispersed in the aggregates. The individual gel pockets are introduced using XFEM soft discontinuities which model the bi-material interface between the gel and the un-reacted aggregate. The geometry of the gel pockets is updated at each step of the simulation, and the enrichment of the mesh recalculated.

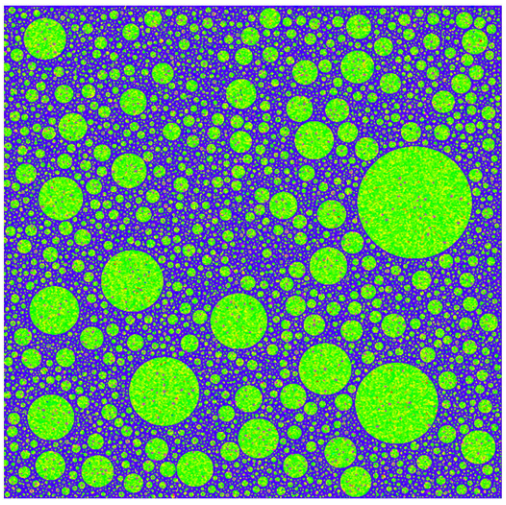

Fig. 1. Simulated slices for 0–16 aggregate size.

3.2.2. Kinetic model

The micro-mechanical model relates expansion to gel amount; the reaction rate, and thus the production of gel was assumed to occur at a fixed rate, which was fit to experimental results. This simplification is justified by the observation of Ben Haha who found that the amount of "reaction", measured by image analysis was roughly linear with time (Fig. 2a). Although the simulations model gel creation, which is different from the "reaction" measured using image analysis, which is more a measure of damage, it was shown that these were linearly related [11] (Fig. 2b). This further implies that any effect of the diffusion of alkali ions in the aggregates is neglected.

3.2.3. Mechanical model

The elastic properties of the gel are assumed to be similar to that of C–S–H. The values of the modulus and the fitting process are described in [16]. The mechanical property of the gel is the only fitting parameter of this model. The expansion of the gel pockets is modelled as a homogeneous strain imposed by forces on appropriate degrees of freedom. This model is a simplification from reality, where the gel is probably visco-elastic. It is however sufficiently detailed to capture the effects of gel localisation. The stress imposed is calculated by assuming that 1 volume of aggregate which reacts is replaced by 2 volumes of gel. This value is obtained by comparing the density of SiO_2 and that of a mineral equivalent of the ASR gel:kanemite, following the work of Kirkpatrick and colleagues [21]. At each step of the simulation, the radius of the gel pockets is increased, and the resulting damage is computed. The stress imposed by the swelling of the gel on a node of the mesh to which is attached the shape function h is, with $\mathbb{E}_{gel}$ the Cauchy-Green stress tensor of the gel and ϵ_{imp} the force from the imposed strain of the gel:

$$\int_{\text{gel volume}} \nabla^T h \mathbb{E}_{gel} \epsilon_{imp} \; dV. \tag{1}$$

To perform the integration over the gel volume, a quadrature is generated by producing a mesh of the gel pocket (radius R and centre x_0, y_0) and the element containing it. The shape functions of the enriched elements are the linear shape functions:

$$\{\xi,\ \eta,\ 1-\xi-\eta\} \tag{2}$$

The enrichment shape functions are:

$$\{\xi|R-r|,\ \eta|R-r|, (1-\xi-\eta)|R-r|\} \tag{3}$$

with r the distance to the centre of the gel pocket.

The behaviour of the materials other than gel (paste and aggregate) is assumed to be elastic–plastic, with a threshold damage which causes the failure of the elements. The area under the stress–strain curves is chosen to match the experimental fracture energy of the paste and the aggregates (from [22]). The discrete weak form of elasticity used to form the stiffness matrix of the problem is per pair of shape functions i,j in an element with d the damage:

$$\int_{V_e} \nabla^T h_i \mathbb{E}_{\text{material}} \left(1-d(\sigma,\epsilon)\right) \nabla h_j \; dV_e. \tag{4}$$

The damage is calculated using a globally energy-minimising algorithm which attributes damage locally. The algorithm works by progressively softening the elements, in the order which is prescribed by their fracture criterion. More details can be found in [23]. This

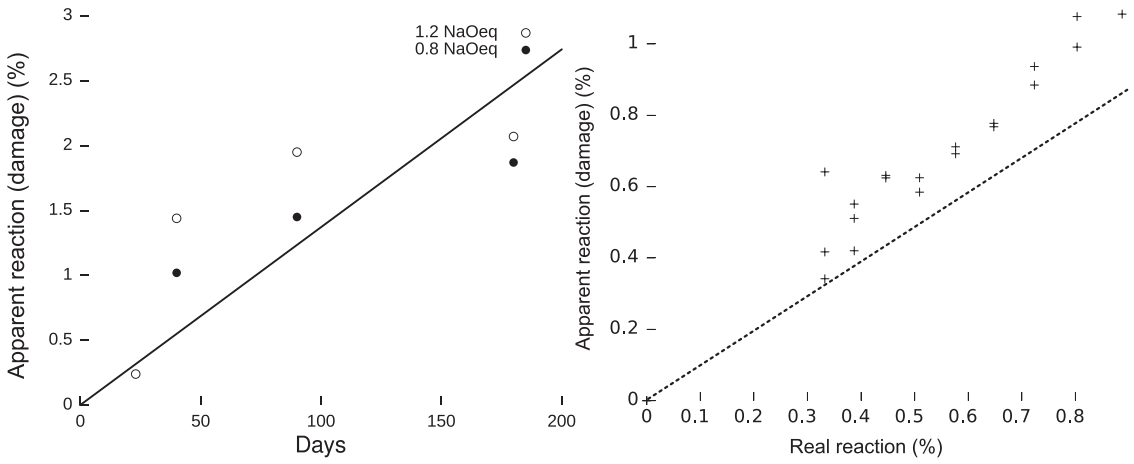

Fig. 2. On the left, damage with time for mortars, adapted from Ben Haha [22]. The drop in damage for the later points is probably due to leaching in Ben Haha's experimental setup. The line is the linear regression line passing through the origin. On the right, correlation between damage and gel production in a mortar simulation.

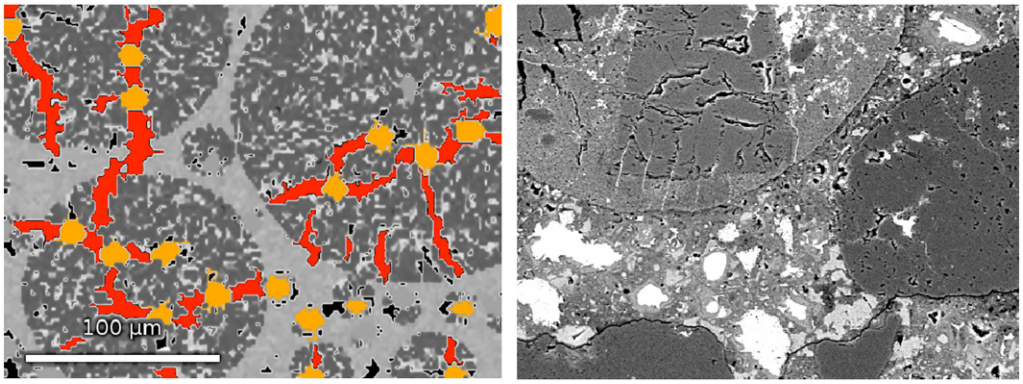

Fig. 3. Detail of a fracture pattern generated by the ASR model (left). For comparison, a micrograph at the same scale of an aggregate (right).

algorithm is designed to capture the damage patterns, which can be compared to experimental observations (Fig. 3): the algorithm exhibits little sensitivity to the loading step. This property is essential as the loading of the sample is caused by the growth of the gel pockets, which is stepped in the simulation, and can amount to large increases in the load between two steps. The mechanical properties used for the simulation are reported in Table 4.

4. Results and discussion

4.1. Experimental results

Expansion results for samples with a single fraction of reactive aggregate are reported in Fig. 4. All mixes have a similar shape of expansion curve: a period in which the expansion accelerates, lasting about 150 days, then a constant expansion rate, and finally a slow-down of the expansion. These different periods can be better discriminated by plotting the rate of expansion, which, although noisy, shows the period of constant expansion quite clearly (grey area).

All mixes seem to both accelerate and start decelerating their expansions at the same time (Fig. 5). The rates of expansion between 150 and 300 days vary with the fraction which is reactive: the 4–8 mm expand the fastest, followed by the 8–16 mm. The 0–2 mm and the 2–4 mm fractions behave identically (Fig. 5). The early phase of the expansion is consistent with results reported by French

Table 4
Mechanical properties of the different materials in the simulation. d_{crit} is the maximum value of the damage before failure, ρ the characteristic distance of the material.

	E_0	ν	$\sigma_{yield,\ c}$	$\sigma_{yield,\ t}$	d_{crit}	ρ
	GPa	–	MPa	MPa	–	mm
Paste	12	0.3	−23.2	2.9	0.95	0.5
Agg.	59	0.3	−45.6	5.7	0.95	0.5
Gel	21.7	0.5	–	–	–	–

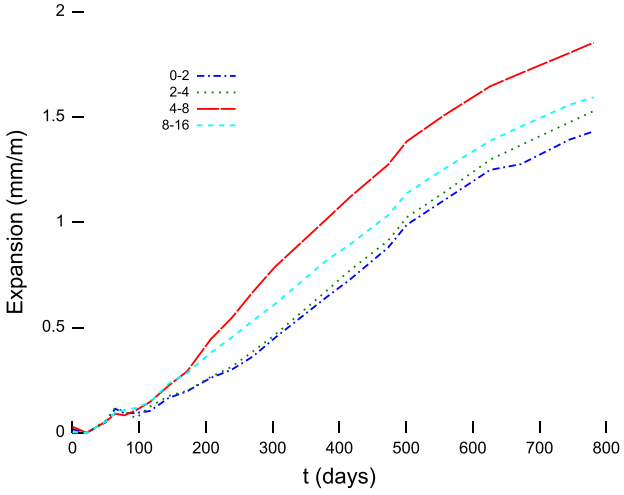

Fig. 4. Expansions of concretes with a single reactive fraction as a function of time.

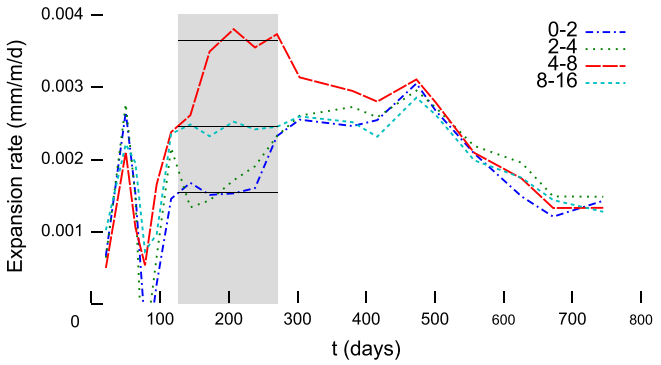

Fig. 5. Expansion rates of concretes with a single reactive fraction as a function of time. The shaded area is the time period used to determine the average rate at the end of the induction period.

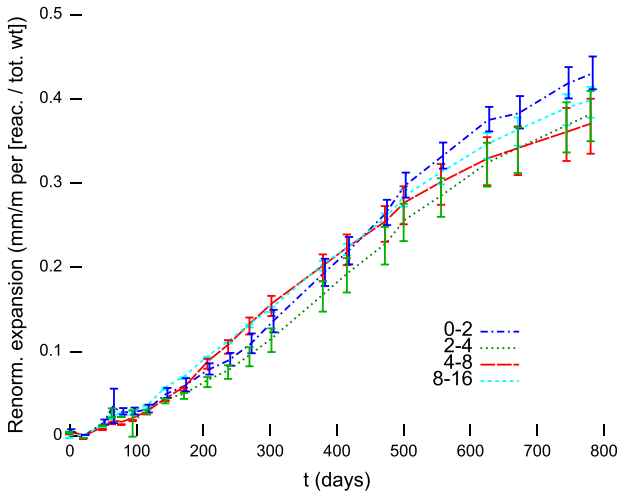

Fig. 6. Expansion rates of concretes with a single reactive fraction as a function of time, normalised for the fraction of reactive material.

and colleagues [5] and Zhang and colleagues [4], with the 4–8 mm giving rise to the most expansion, followed by the 8–16 mm.

The slow-down of the expansions occurs at the same time. As the samples were cured in sodium hydroxide solutions, the only limitation to the reaction should be the reactive material provided by the aggregates. When the expansions are normalised for the weight fraction of reactive material, it appears that the expansions are significantly different only in the early stages of the reaction. In the longer term, the extent of the expansion is identical for all reactive fractions considered (Fig. 6). Microscopic observations show ASR gel forms in pockets dispersed throughout the aggregate volume: although the number of pockets vary with the aggregate volume, their individual size is relatively constant as it depends on mineralogy. Therefore, it is reasonable to assume that all gel pockets react at the same rate.

These observations suggest a complex relation between the degree of reaction in the aggregates and the cracking and expansion of the material. To study these links, a numerical modelling approach was used.

4.2. Numerical modelling

Previous experimental studies using BSE microscopy of slow-reacting aggregates found relatively few cracks in the cement paste when the aggregates were already significantly cracked [13].

The first approach was to use single aggregates embedded in a cement-like matrix (Fig. 7). The simulations were performed in non-periodic boundary conditions, with only a pin and a roller used to inhibit free body movements. The results showed that without external loads, the expansion happens in two phases: first, the damage is confined within the aggregates, and the deformation of the surrounding paste is essentially elastic. In the second phase, cracks propagate in the paste, and much larger expansions are observed. The expansions of the single aggregate samples before the onset of paste cracking (normalised for the amount of gel per aggregate) are plotted in Fig. 9 and compared to the experimental observations (normalised for the fraction of reactive aggregate).

Fig. 8 shows the expansion versus reaction curve normalised to the volume of single aggregates up to the point where cracks penetrate the paste. At that point, as there is no restraint, the cracks grow uncontrollably. The rate used in Fig. 9 is the rate observed on the step preceding the penetration of the crack into the paste. The same trends are observed in simulations and experiments, with the rate depending on the aggregate size.

The expansions recorded are very low because they concern a single aggregate and not a complete microstructure. In a complete microstructure the paste is under compression from all the aggregates expanding, and the softening of the aggregates translates into a macroscopic slow-down of the expansion. No such mechanism exists in single aggregate simulations. However, the crack propagation within the aggregate is little affected by the compression of the paste, which is in the order of megaPascals, because it is driven by the stress induced by gel pockets, which is in the order of gigaPascals.

Simulations of full samples were also performed for selected fractions. The simulations were run until the damage reached the paste as the available memory on the computers used did not allow for very

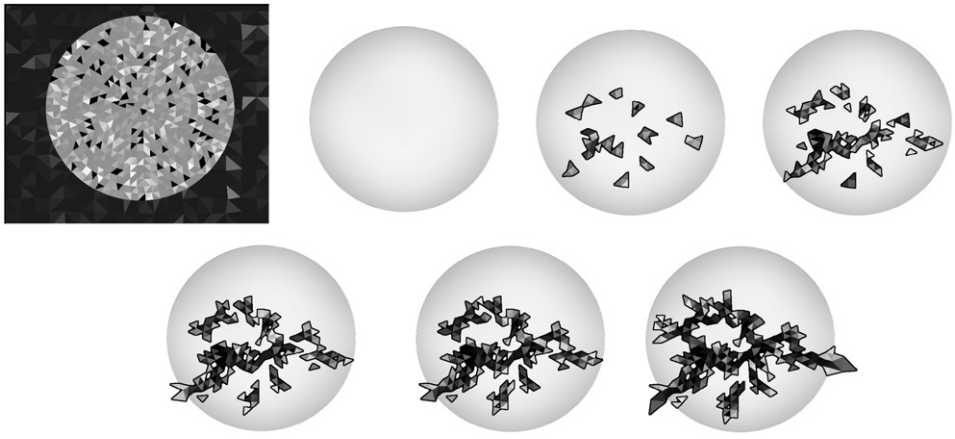

Fig. 7. Montage of the progressive formation of a crack network in a single inclusion. States at the bottom right show cracked paste.

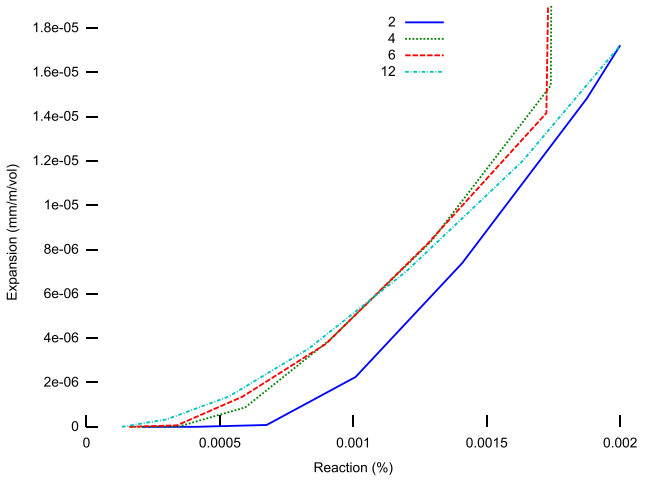

Fig. 8. Expansion-reaction curves for single aggregates up to the point when cracks penetrate the paste. The expansions are in mm/m, renormalised by the area of the aggregate. The x axis is in % of the aggregate transformed into gel. This quantity can be assumed to be linear with time.

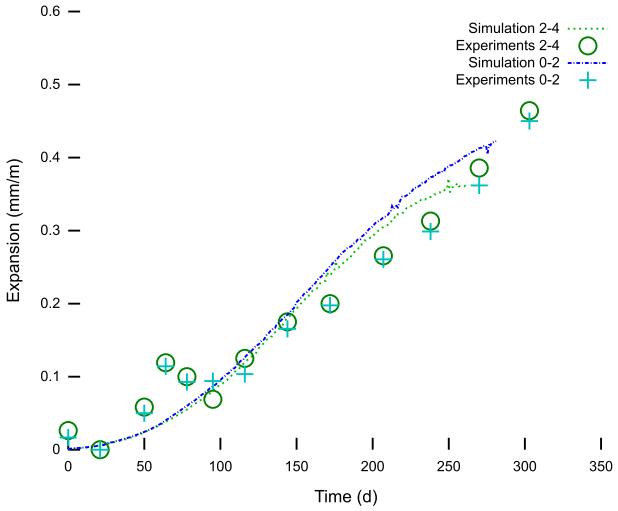

Fig. 10. Simulated and real expansions of the 0–2 and 2–4 fractions.

fine meshing of both the paste and the aggregates. The samples simulated were those with the reactive 0–2 mm and 2–4 fractions, as there is twice as much reactive material in the 0–2 mm fraction as in the 2–4 mm fraction, but the expansions are almost the same. The resulting expansion curves are plotted in Fig. 10.

The two samples exhibit very similar expansions despite the 0–2 mm having twice the number of expansive gel pockets. The effect of more reactive material is almost perfectly compensated by the fracture mechanics of the aggregates. Damage also reaches the paste at almost the same time in both samples (Fig. 11). The contrast in the figure has been adjusted to highlight the damage in the paste. The dark zones in the aggregates are also damaged, which occurred at earlier steps of the simulation. It can be seen that only aggregates with diameters between 2 and 4 mm are damaged, and that damage in the paste occurs preferentially where they form clusters. The location of the damage in the paste may be the consequence of the 2D nature of the simulation.

This numerical study and previous microscopic observations show that the failure is caused by the development of a network of cracks. The difference in expansion rates measured and reproduced through numerical simulation indicate that the macroscopic expansion during that period is dependant on the size-dependant cracking behaviour of aggregates. This is consistent with the analytic study by Reinhardt and colleagues which showed that there is a size-dependent critical crack length which causes the failure of the individual aggregate [12]. When the cracks reach the paste, however, their propagation depends only on the fracture properties of the latter. The macroscopic rate of expansion then does not depend on the size of the reactive aggregates, but only on the global PSD.

5. Conclusion and perspectives

The ASR micro-mechanical model was found to be a useful tool to gain insights in the mechanisms of ASR induced degradation in the case of single reactive fractions. The effects of individual size fractions were related to the failure behaviour of individual aggregates. This suggests that the expansion curves of ASR affected concretes are the product of three different causes. First, the expansion is caused by the cracking of the aggregates and the elastic deformation of the paste. Then during a transition period, both aggregate and paste cracking drive the expansion. Finally, the expansion is driven by paste cracking and the exhaustion of reactive materials. Laboratory studies on slowly-

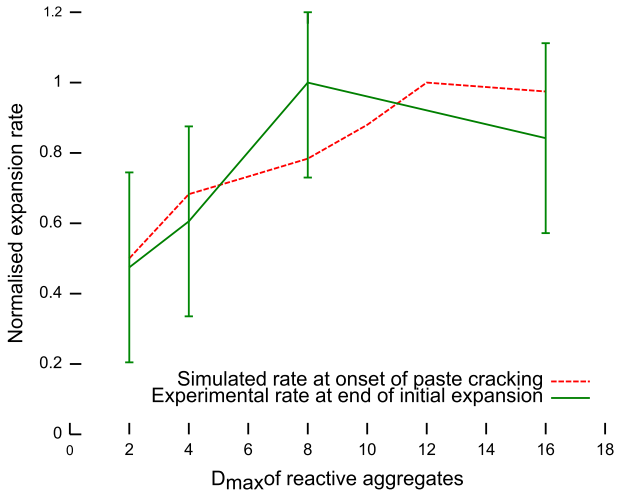

Fig. 9. Expansion rates of samples with a single reactive fraction and expansion of samples with a single reactive aggregate as a function of the D_{max}.

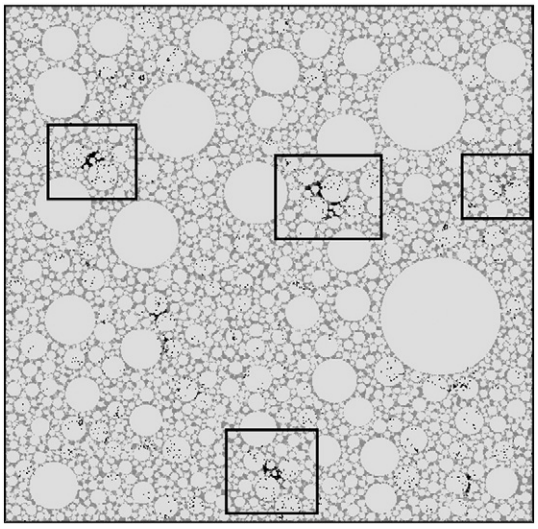

Fig. 11. Damage patterns in the paste at the end of the simulation. The black boxes mark some of the damaged zones. Dark spots in the paste and aggregates mark the location of damage.

reactive aggregates exhibit typically low expansions, as only the first and second phases occur within the time-frame of the experiment. Studies on rapidly-expanding aggregates may on the contrary miss the first phases, and result in expansion curves which depend mostly on the mechanical properties of the cement.

Acknowledgements

The authors are grateful to the Swiss Federal Office for Energy (OFEN) and the Swiss National Science Foundation (grants PA00P2-139671 and PBELP2-130912) for their support, financial and otherwise.

References

[1] S. Poyet, A. Sellier, B. Capra, G. Foray, J.M. Torrenti, H. Cognon, E. Bourdarot, Chemical modelling of alkali silica reaction: influence of the reactive aggregate size distribution, Mater. Struct. 40 (2) (2007) 229–239.
[2] M. Cyr, P. Rivard, F. Labrecque, Reduction of ASR-expansion using powders ground from various sources of reactive aggregates, Cem. Concr. Compos. 31 (7) (2009) 436–446.
[3] K. Ramyar, A. Topal, Ö. AndiÄ¯, Effects of aggregate size and angularity on alkali–silica reaction, Cem. Concr. Res. 35 (11) (2005) 2165–2169.
[4] C. Zhang, A. Wang, M. Tang, B. Wu, N. Zhang, Influence of aggregate size and aggregate size grading on ASR expansion, Cem. Concr. Res. 29 (2009) 1393–1396.
[5] W.J. French, Avoiding concrete aggregate problems, Improving Civil Engineering Structures—Old and New, Geotechnical Publishing Ltd, 1994, pp. 65–95.
[6] P.A. Dahl, J. Lindgård, S.W. Danielsen, C. Hagby, R. Kompen, B. Pedersen, T.F. Rønning, Specifications and guidelines for production or AAR resistant concrete Norway, 12th ICAAR, 2004, pp. xxx – xxx.
[7] B.J. Wigum, Alkali-aggregate reactions in concrete: properties, classification and testing of Norwegian cataclastic rocks, University of Trondheim, Properties of Alkali-Reactive Aggregates, 1995, pp. 22–43.
[8] B.J. Wigum, W.J. French, R.J. Howarth, C. Hills, Accelerated tests for assessing the potential exhibited by concrete aggregates for alkali-aggregate reaction, Cem. Concr. Compos. 19 (5) (1997) 451–476.
[9] Z.P. Bažant, A. Steffens, Mathematical model for kinetics of alkali–silica reaction in concrete, Cem. Concr. Res. 30 (3) (1999) 419–428.
[10] S. Multon, N. Leklou, L. Petit, Coupled effects of aggregate size and alkali content on ASR expansion, Cem. Concr. Res. 38 (3) (2008) 350–359.
[11] C.F. Dunant, Experimental and modelling study of the alkali–silica-reaction in concrete, Ph.D. thesis, École Polytechnique Fédérale de Lausanne (2009).
[12] H.W. Reinhardt, O. Mielich, A fracture mechanics approach to the crack formation in alkali-sensitive grains, Cem. Concr. Res. 41 (3) (2010) 255–262.
[13] M. Ben Haha, E. Gallucci, A. Guidoum, K.L. Scrivener, Relation of expansion due to alkali silica reaction to the degree of reaction measured by SEM image analysis, Cem. Concr. Res. 37 (8) (2007) 1206–1214.
[14] J. Bolomey, Granulation et prévision de la résistance probable des bétons, Travaux 30 (19) (1935) 228–232.
[15] B. Lothenbach, F. Winnefeld, Thermodynamic modelling of the hydration of Portland cement, Cem. Concr. Res. 36 (2005) 209–226.
[16] C. Dunant, P.N. Vinh, M. Belgasmia, S. Bordas, A. Guidoum, Architecture tradeoffs of integrating a mesh generator to partition of unity enriched object-oriented finite element software, Rev. Eur. Méc. Numér. 16 (2007) 237–258.
[17] C.F. Dunant, K.L. Scrivener, Micro-mechanical modelling of alkali–silica-reaction-induced degradation using the AMIE framework, Cem. Concr. Res. (4) (2010) 517–525.
[18] C.F. Dunant, K.L. Scrivener, Effects of uniaxial stress on alkali–silica reaction induced expansion of concrete, Cem. Concr. Res. 42 (2012) 567–576.
[19] G. Bach, Über die größenverteilung von kugelschnitten in durchsichtigen schnitten endlicher dicke, Z. Angew. Math. Mech. 38 (7–8) (1959) 256–258.
[20] P.L. Goldsmith, Calculation of true particle size distributions from the sizes observed in a thin slice, the, Br. J. Appl. Phys. 18 (6) (1967) 813–830.
[21] R.J. Kirkpatrick, A. G. K., X. Hou, L. Struble, Experimental and molecular dynamics modeling studies of interlayer swelling: water incorporation in kanemite and ASR gel, Mater. Struct. 38 (2005) 449–458.
[22] M. Ben Haha, Mechanical effects of alkali silica reaction in concrete studied by SEM-image analysis, Ph.D. thesis, École Polytechnique Fédérale de Lausanne (May 2006).
[23] C.F. Dunant, P. Kerfriden, S. Bordas, K.L. Scrivener, T. Rabczuck, An algorithm to compute damage from load in composites, Front. Archit. Civil Eng. Chin. 5 (2) (2011) 180–193.
[24] T.E. Stanton, Expansion of concrete through reaction between cement and aggregate, Proc. Am. Soc. Civil Eng. 66 (10) (1940) 1781–1811.